VIRTUAL RESISTIVE NETWORK AND CONDUCTIVITY RECONSTRUCTION WITH FARADAY'S LAW

MIN GI LEE, MIN-SU KO, AND YONG-JUNG KIM

Abstract. Network based conductivity reconstruction method is introduced using the third Maxwell's equation, or Faraday's law, for a static case. The usual choice in electrical impedance tomography is the divergence free equation of the electrical current density. However, if the electrical current density is given, the curl free equation of the electrical field gives a direct relation between the current and conductivity and this relation is used in this paper. Mimetic discretization is applied to the equation, which gives the virtual resistive network system. Properties of the introduced numerical schemes are investigated and its advantage over other conductivity reconstruction methods is discussed. Numerically simulated results with an analysis of noise propagation are presented.

1. Introduction

Suppose that $\Omega \subset \boldsymbol{R}^d, d \geq 2$, is a bounded simply connected domain of an electrical conductivity body with a smooth boundary $\partial\Omega$ and $r_0 : \Gamma \subset \partial\Omega \to \boldsymbol{R}^+$ is a given boundary resistivity. The purpose of this paper is to develop a numerical algorithm to find the isotropic resistivity distribution $r : \Omega \to \boldsymbol{R}^+$ that satisfies

$$\begin{aligned} &\nabla \times (r\mathbf{F}) = 0 \ \text{ in } \ \Omega, \\ &r = r_0 \ \text{ on } \ \Gamma \subset \partial\Omega, \end{aligned} \tag{1.1}$$

when a single set of current density $\mathbf{F} : \Omega \to \boldsymbol{R}^d$ and a boundary resistivity r_0 on $\Gamma \subset \partial\Omega$ are given. This curl free equation is the third Maxwell's equation, or Faraday's law, for the static electromagnetism. The existence of such resistivity is clear if $\mathbf{F}$ is an exact current density generated by an isotropic conductivity body. However, the existence fails for a general vector field. It has been shown in two space dimension that, if the vector field $\mathbf{F}$ and the boundary Γ are admissible in the sense of Definition 2.1, such a resistivity distribution exists and is unique (see [19, Theorem 1]).

This problem is from a magnetic resonance imaging based electrical impedance tomography problem or MREIT for brevity (see [11, 14, 24, 27, 28]). For example, if an injection current is applied to the boundary of a conductivity body, the voltage u satisfies the following divergence free equation

$$\begin{aligned} &\nabla \cdot (\sigma \nabla u) = 0 \qquad \text{in } \Omega, \\ &-\sigma \nabla u \cdot \mathbf{n} = g \qquad \text{on } \partial\Omega, \end{aligned} \tag{1.2}$$

where $\sigma = r^{-1}$ is the conductivity, $\mathbf{n}$ is the outward unit normal vector to the boundary $\partial\Omega$, and g is the normal component of the boundary current that satisfies $\int_{\partial\Omega} g ds = 0$. Then, the current density $\mathbf{J}$ and the voltage u satisfy Ohm's law:

$$\mathbf{J} = -\sigma \nabla u \quad \text{in } \Omega. \tag{1.3}$$

The system (1.2)–(1.3) has been used to construct the conductivity σ in an iterative way when a current density $\mathbf{J}$ is given (see [15, 18] and Appendix A). However, we may construct the conductivity directly by choosing Faraday's law (1.1) since the conductivity and the electrical current are explicitly involved in this equation. In this way we may avoid the convergence issue caused by iterative arguments and obtain faster reconstruction algorithm.

If the conductivity σ is a $d \times d$ symmetric or diagonal matrix, it is called an anisotropic or orthotropic conductivity, respectively. We are interested in an isotropic conductivity case in this paper which is a scalar valued one. Finding the conductivity image has been one of central issues of inverse problems. The electrical impedance tomography (or EIT) is now a classical example (see [1, 2, 5, 10] and references therein). The conductivity image is constructed in EIT from boundary measurements of voltage and the elliptic equation (1.2) gives a direct relation between the voltage and the conductivity. The uniqueness of the conductivity σ that satisfies (1.2) for all possible boundary measurements is known for the isotropic case in two and three space dimensions (see [23, 26]). However, for an anisotropic conductivity case, the uniqueness is only given in equivalence classes by diffeomorphisms (see [10]). The uniqueness of the conductivity that satisfies (1.2)–(1.3) for a given current density $\mathbf{J}$ is well known when two sets of current density are given [16] or a single set of current density is given with the boundary voltage or resistivity [13, 17, 22].

The existence of the conductivity σ that satisfies (1.2) is usually assumed, but hardly studied, in conductivity reconstruction problems since the data is supposed to be obtained from an existing conductivity body. However, if the data contain a noise, the existence should be the main concern and hence the first step is to specify a class of data that allows the existence. The admissibility condition in Definition 2.1 has been introduced to classify current data that provide the existence of a corresponding conductivity. It is known that inverse problems are exponentially instable and EIT is a well known example. Recently the limitation of obtainable resolution has been studied for linearized EIT problems by Ammari *et al.* [3, 4]. For MREIT problems the Hölder conditional stability of (1.2) and the stability of its linearized problem has been studied in [21, 22]. The stability of the conductivity reconstruction of the original nonlinear MREIT problem has been obtained within the class of admissible current data by Kim and Lee [19].

In this paper we develop a numerical algorithm which is based on a virtual resistive network system (or VRN for brevity). For simplicity, we construct a rectangular VRN in this paper. However, the algorithm comes from a contour integration of an arbitrary network system and one may develop various shapes of network system depending on the geometry of a given problem. Since the network system plays as a background of the discretization, one may rotate it as in Figure 8 and obtain various reconstructed images. This reconstruction algorithm has a nature of hyperbolic problems such as the noise propagation along characteristics and the domains of dependence and influence (see Figures 5 and 6). The computational cost of the algorithm is very low since the conductivity is obtained from a cell by cell local computation. Hence, its extension to the three dimensions is promising.

Since the VRN method is a non-iterative method, its numerical simulation has been compared with two other non-iterative methods, the equipotential line and direct integration methods [12, 13, 17]. All the computations are done with a single set of current data. The key of the conductivity reconstruction is to reduce the noise propagation along characteristic lines which is the source of noisy stripes in the reconstructed images. The VRN method reduces the appearance of such stripes. However, if the noise level becomes as big as 40%, such stripes still appear as in Figure 17. One may develop various shapes of network system (see [20]) or apply two sets of current data with perpendicular characteristic lines to reduce the appearance of the noisy stripes. A widely used reconstruction method in MREIT is the harmonic B^z algorithm [24], which is an iterative method. A comparison with the method is given in Appendix A. One can similarly observe the stripes of noise in Figure 19. However, if two electrical current density are used, the image is improved considerably.

2. A mimetic approach for the Maxwell-Faraday equation

Let $\Omega \subset \boldsymbol{R}^2$ be a bounded simply connected domain of a conductivity body and its boundary $\partial\Omega$ be smooth. We consider a static electromagnetic field $\mathbf{E}$ in the body. First, the *electric field* satisfies

$$\nabla \times \mathbf{E} = 0, \tag{2.1}$$

which is the static Maxwell-Faraday equation. Therefore, there exists a *potential* u (or *voltage*) that satisfies

$$\mathbf{E} = -\nabla u.$$

Let $\sigma : \Omega \to \boldsymbol{R}^+$ be an *isotropic conductivity* distribution of the body and $r = \sigma^{-1}$ be its inverse which is called the *resistivity* distribution. We assume that σ and r are bounded away from zero. The *current density* $\mathbf{J}$ is given by Ohm's law:

$$\mathbf{J} = \sigma\mathbf{E} \quad \text{or} \quad \mathbf{E} = r\mathbf{J}. \tag{2.2}$$

We will denote the exact current density by $\mathbf{J}$ and a one with a noise by $\mathbf{F}$. If a vector field $\mathbf{F}$ does not contain any noise, i.e., $\mathbf{F} = \mathbf{J}$, there exists at least one resistivity distribution r that satisfies

$$\begin{aligned} &\nabla \times (r\mathbf{F}) = 0 \ \text{ in } \ \Omega, \\ &r = r_0 \ \text{ on } \ \Gamma \subset \partial\Omega, \end{aligned} \tag{2.3}$$

which is the one that produced the given current. However, the uniqueness of such resistivity fails if the boundary Γ does not cover enough region. Furthermore, if the given current density $\mathbf{F}$ contains a noise, the existence part is not guaranteed, neither. Hence, we should classify vector fields $\mathbf{F}$ and the correct portion of the boundary $\Gamma \subset \partial\Omega$ that allows the existence and the uniqueness.

Definition 2.1. *Consider a two dimensional vector field* $\mathbf{F} = (f^1, f^2) \in C^{1,\alpha}(\overline{\Omega})$ *for* $\alpha > 0$. *Denote* $\Gamma^+ := \{\mathbf{x} \in \partial\Omega \,|\, \mathbf{F}^\perp \cdot \mathbf{n}(\mathbf{x}) > 0\}$, $\Gamma^- := \{\mathbf{x} \in \partial\Omega \,|\, \mathbf{F}^\perp \cdot \mathbf{n}(\mathbf{x}) < 0\}$, $\Gamma^0 := \{\mathbf{x} \in \partial\Omega \,|\, \mathbf{F}^\perp \cdot \mathbf{n}(\mathbf{x}) = 0\}$ *and* $\Omega' := \overline{\Omega} \setminus \Gamma^0$, *where* $\mathbf{F}^\perp := (-f^2, f^1)$ *(see Figure 1). The vector field* $\mathbf{F}$ *is called admissible if* $\mathbf{F} \neq 0$ *in* $\overline{\Omega}$ *and* $\Gamma^\pm$ *are connected. The two connected boundaries,* $\overline{\Gamma^+}$ *and* $\overline{\Gamma^-}$, *are called admissible boundaries.*

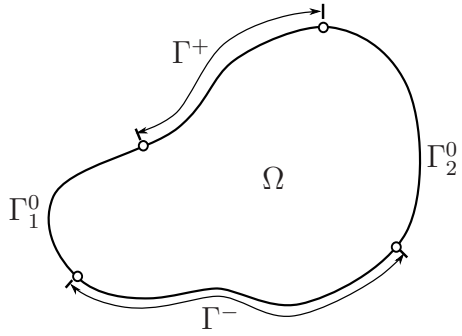

FIGURE 1. Domain Boundary: The boundary of the domain is divided into four parts depending on the given admissible vector field $\mathbf{F}$ in the sense of Definition 2.1.

It has been shown that there exits a unique resistivity distribution $r : \Omega \to \boldsymbol{R}^+$ that satisfies (2.3) if the vector field $\mathbf{F}$ and the boundary Γ are admissible (see [19]). Furthermore, the resistivity r is perturbed stably under a perturbation of the vector field $\mathbf{F}$ and the boundary condition r_0 as long as the pair $\mathbf{F}$ and Γ are admissible. It is also shown that one may construct an admissible current density $\mathbf{J}$ for any given conductivity σ by choosing a boundary current properly.

In the rest of this paper we will develop a numerical algorithm that constructs the resistivity r from a given admissible data $\mathbf{F}$. One of the simplest method is to discretize (2.3) using a finite difference method (see Remark 3.2). The construction of the resistivity distribution is sensitive to noise and minimizing the computation error is critical in obtaining a better resistivity image. In this paper we will use the idea of resistive network system and Kirchoff's voltage and current laws. This idea turns out to be an example of mimetic discretization of the curl equation. Readers are referred to [6, 7, 8, 9] for more information about mimetic discretization.

In mimetic discretization the potential u is assigned at vertices. Consider rectangular mesh $(x^i, y^j) \in \boldsymbol{R}^2$ with $0 \le i, j \le n$ in Figure 2. The potential values are assumed to approximate $u^{ij} \cong u(x^i, y^j)$ (see Figure 2(a)). On the other hand, vector fields such as the current density $\mathbf{J}$ or the electrical field $\mathbf{E}$ is assigned along edges. For example, $E^{i+\frac{1}{2}j}$ is the component of the electrical field $\mathbf{E}$ in the direction connecting two mesh points (x^i, y^j) and (x^{i+1}, y^j). Notice that $(x^{i+\frac{1}{2}}, y^j)$ denotes the midpoint of this edge. Then, we may set

$$E^{i+\frac{1}{2}\,j} = -\frac{u^{i+1\,j} - u^{i\,j}}{x^{i+1} - x^i}, \qquad E^{i\,j+\frac{1}{2}} = -\frac{u^{i\,j+1} - u^{i\,j}}{y^{j+1} - y^j} \tag{2.4}$$

(see Figure 2(b)). The conductivity and the resistivity are given by Ohm's Law, $\mathbf{J} = \sigma\mathbf{E}$ or $\mathbf{E} = r\mathbf{J}$. Therefore, it is natural to assign them along the edges. Hence, we set

$$\begin{aligned} J^{i+\frac{1}{2}\,j} &= \sigma^{i+\frac{1}{2}\,j} E^{i+\frac{1}{2}\,j}, \\ J^{i\,j+\frac{1}{2}} &= \sigma^{i\,j+\frac{1}{2}} E^{i\,j+\frac{1}{2}}, \end{aligned} \quad \text{or} \quad \begin{aligned} E^{i+\frac{1}{2}\,j} &= r^{i+\frac{1}{2}\,j} J^{i+\frac{1}{2}\,j}, \\ E^{i\,j+\frac{1}{2}} &= r^{i\,j+\frac{1}{2}} J^{i\,j+\frac{1}{2}}. \end{aligned} \tag{2.5}$$

If $\mathbf{F}$ is divergence free, i.e., $\nabla \cdot \mathbf{F} = 0$, then it is convenient to consider a *stream function* ψ that satisfies

$$\mathbf{F} = \nabla^{\perp}\psi, \quad \text{where } \nabla^{\perp} := \begin{pmatrix} \partial_y \\ -\partial_x \end{pmatrix}.$$

The value of the stream function is assigned to the midpoint of each cell, i.e., $\psi^{i+\frac{1}{2}\,j+\frac{1}{2}} \cong \psi(x^{i+\frac{1}{2}}, y^{j+\frac{1}{2}})$(see Figure 2(c)). Then, $\mathbf{F}$ is given by

$$F^{i+\frac{1}{2}j} = \frac{\psi^{i+\frac{1}{2}\,j+\frac{1}{2}} - \psi^{i+\frac{1}{2}\,j-\frac{1}{2}}}{y^{j+\frac{1}{2}} - y^{j-\frac{1}{2}}}, \qquad F^{ij+\frac{1}{2}} = -\frac{\psi^{i+\frac{1}{2}\,j+\frac{1}{2}} - \psi^{i-\frac{1}{2}\,j+\frac{1}{2}}}{x^{i+\frac{1}{2}} - x^{i-\frac{1}{2}}}. \tag{2.6}$$

If $\nabla \cdot \mathbf{F} \neq 0$, we will take the divergence free part of the Helmholtz decomposition of the field $\mathbf{F}$.

This mimetic approach is identical to the resistive network system given in Figure 3. This resistive network has been virtually made from a continuum body as a discretization method, which is the reason why we call it a *virtual resistive network* (or VRN for brevity). The use of mimetic discretization reduces computation error. For example, the sum of edge values of $\mathbf{E}$ along any closed loop in the network automatically becomes zero, which is not the case of a finite difference method. In other words, Kirchoff's law of voltage is exactly satisfied and hence the main part of the computation error is from the data, but not from the discretization of the problem.

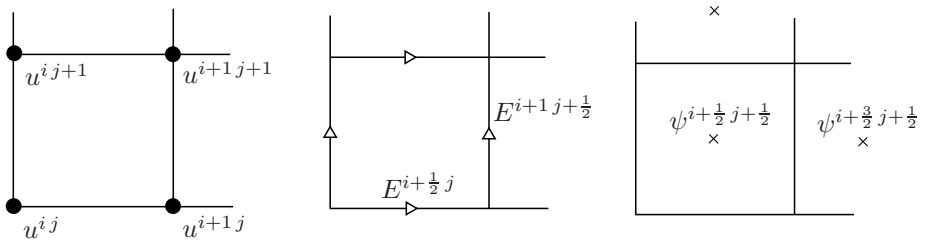

(a) potential function (b) vector field (c) stream function

FIGURE 2. Mimetic discretization: The potentials are assigned at vertices, the electrical fields are assigned along the edges, and stream functions are in cells.

3. Rectangular VRN

We now derive a conductivity reconstruction algorithm using a rectangular uniform VRN and investigate its property. This rectangular network system gives basic properties of the algorithm clearly and easily. However, one may develop other shapes of VRN to improve its performance. In fact, one of the main advantages of mimetic approach is that it handles non-uniform discretization equally well. For a presentational simplicity we consider a rectangular domain $\Omega = (0,1) \times (0,1)$ and the boundary $\Gamma = \{0\} \times [0,1] \cup [0,1] \times \{0\} \subset \partial\Omega$. However, one may handle any shape of domain by simply placing it on the rectangular VRN. In fact, the simulations in Section 5 are for a circular domain placed on the rectangular network developed in this section. The mesh points (x^i, y^j) are

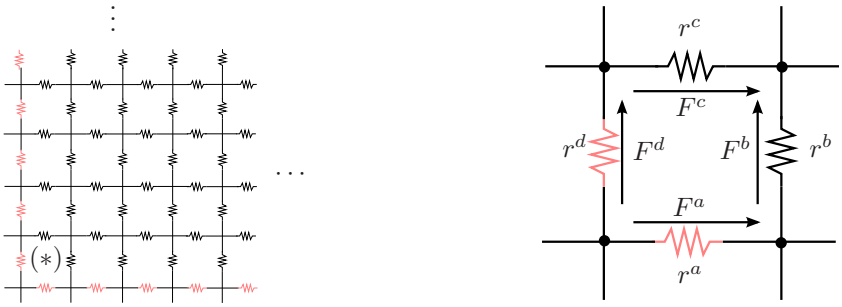

(a) rectangular VRN (b) components of a cell

FIGURE 3. A rectangular network. If the resistivity values of boundary resistors along two sides of the rectangular domain, the colored (or grey) ones, are given, the others can be computed by a cell by cell local computation.

with $0 \le i, j \le n$. Hence there are $(n+1)^2$ vertices, $2n(n+1)$ edges, and n^2 cells. We assume that the boundary resistivity r_0 is given along the edges on the boundary Γ (see Figure 3(a)). In other words, $2n$ number of resistors are given initially and therefore, our job is to decide the other $2n^2$ resistors.

Let D be the area of a cell (see Figure 3(b)). Then, the integration of (2.3) over the area D gives

$$0 = \int_D \nabla \times (r\mathbf{F}) dx = \oint_{\partial D} r\mathbf{F}(z) dz.$$

We will assume that each edge has the same length. Then, the resistor and resistivity are equivalent. For a notational simplicity, we denote the resistor and the current density as in Figure 3(b). Then, the above equation is written as

$$r^a F^a + r^b F^b - r^c F^c - r^d F^d = 0, \tag{3.1}$$

which is also called Kirchoff's voltage law. Note that there are n^2 number of cells and hence n^2 equations. Therefore the number of equations are not enough to decide $2n^2$ unknown resistors. If two sets of current data are given, say $\mathbf{F}_1$ and $\mathbf{F}_2$, then we obtain $2n^2$ equations and those unknowns can be decided. In that case the resistor r^c gives a conductivity in horizontal direction and r^b in vertical direction. In other words, we may actually obtain orthotropic conductivity. For our *isotropic* case, we assume

$$r^b = r^c. \tag{3.2}$$

Then, the total number of unknowns are n^2. Suppose that two resistors r^a and r^d have been obtained in previous steps or initially. One can find such a cell from Figure 3(a), which is at the left bottom corner. Then, the above relation gives

$$r^b = \frac{r^d F^d - r^a F^a}{F^b - F^c} \quad \text{if} \quad F^b \neq F^c. \tag{3.3}$$

If r^b and r^c are obtained, then we have another cell with two given resistors and hence we may continue and find all resistors. Notice that, if $F^b - F^c \cong 0$, we cannot obtain the resistivity correctly. The admissibility condition is actually related to avoid such a situation (see Section 3.1).

Remark 3.1 (Anisotropic Resistivity)**.** *An anisotropic resistivity is a case when the resistivity is a symmetric matrix $r = (r_{ij})$. An orthotropic case is when it is a diagonal matrix, where the r^b and r^c in Figure 3(b) represent the diagonal components. The assumption (3.2) restricts the orthotropic case to the isotropic case.*

Remark 3.2 (VRN versus FDM)**.** *A simple and natural idea to discretize the Maxwell-Faraday equation (1.1) is to apply a finite difference method. If we apply the central scheme, then the approximation of the curl equation at a vertex (x^i, y^j) is*

$$\frac{r^{i+1\,j}F_2^{i+1\,j} - r^{i-1\,j}F_2^{i-1\,j}}{x^{i+1} - x^{i-1}} - \frac{r^{i\,j+1}F_1^{i\,j+1} - r^{i\,j-1}F_1^{i\,j-1}}{y^{j+1} - y^{j-1}} = 0,$$

where $\mathbf{F} = (F_1, F_2)$. This relation has the same structure as the network relation (3.1). The difference is that the network method uses the information more compactly and can be easily applied even for non-rectangular network systems. We will also see that the network approach gives us a better understanding of the reconstruction algorithm.

3.1. **Admissibility of boundary condition.**

Now we study the property of the rectangular VRN. We consider the rectangular domain $\Omega = (0,1)\times(0,1)$ and the boundary $\Gamma = \{0\}\times[0,1]\cup[0,1]\times\{0\}$ for the boundary condition. This choice of boundary allows the existence of a cell with two given resistors (r^a and r^d in Figure 3(b)) all the time. If a different boundary is chosen, then the algorithm should be modified appropriately. In the following discussion we fix the boundary Γ and consider the effect of the direction of currents.

Notice that, if $F^b - F^c \cong 0$ in (3.3), we cannot obtain the resistivity. The admissibility condition in Definition 2.1 is related to avoiding such a situation. For example, the condition $\mathbf{F} \neq 0$ gives the minimum requirement to avoid the case. The boundary Γ^0 is the place for current injection. In our example with $\Gamma = \{0\} \times [0,1] \cup [0,1] \times \{0\}$, the corresponding Γ^0 consists of two points $(0,1)$ and $(1,0)$ and hence the main direction of current is the one connecting these two points. Hence the chance to have $F^b - F^c \cong 0$ is relatively small if the current data $\mathbf{F}$ is admissible.

In Figure 4 three examples of recovered conductivity are given. The boundary Γ is fixed as above and three different current densities are considered, where the currents were injected through two electrodes on the boundary denoted with arrows in the figures. The case of Figure 4(c) is the only case that the boundary Γ is admissible. Note that the conductivity has been reconstructed completely only for this case. This example explains the importance of having an admissible boundary and current density in reconstructing the conductivity.

3.2. **Domain of dependence and influence.**

In the construction algorithm the conductivity of a given cell is obtained after a series of cell by cell computations. In the algorithm the conductivity at a given cell is decided by the cells on its left and below. We may call this region the *domain of dependence* of the conductivity at $\mathbf{x}$ (see Figure 5(a)). Therefore, the noise of current data in this region is the source of the error of the conductivity at $\mathbf{x}$. Similarly, the noise at a give cell propagates to the cells on its right and above. We may call this region the *domain of influence* of the information at $\mathbf{x}$ (see Figure 5(b)).

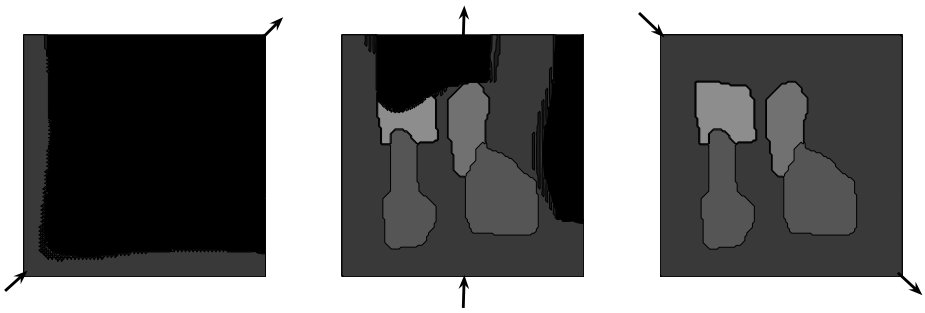

(a) nothing recovered (b) partly recovered (c) fully recovered

FIGURE 4. Two dimensional isotropic conductivity has been recovered with $\Omega = (0,1) \times (0,1)$ and $\Gamma = \{0\} \times [0,1] \cup [0,1] \times \{0\}$. Injection currents are applied through two electrodes denoted by arrows. The boundary Γ is admissible only for the case (c) and the conductivity is fully recovered. Noise is not added in these examples.

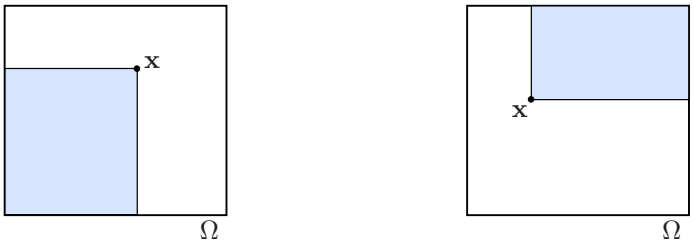

(a) domain of dependence (b) domain of influence

FIGURE 5. The domain of dependence of a conductivity value and the domain of influence of the data at a point $\mathbf{x} \in \Omega$ are in the figures. The show a hyperbolic nature in the curl equation (2.3).

The domains of dependence and influence represent a hyperbolic nature of the problem. A wider region of dependence allows a chance to get a noise mixed and dissipate. Later we will see that, if the network is parallel to characteristic lines, the domains of dependence and influence make a stripe along the characteristic line and the recovered image also consists of many stripes of noise. Hence, it is important to design a network in a way to avoid such a situation.

3.3. **Characteristic lines.**

We may treat the boundary Γ as the image of a curve $\Gamma : [0,1] \to \partial\Omega$. Define $\mathbf{x} : \tilde{\Omega} \subset [0,1] \times \boldsymbol{R}^+ \to \Omega$ such that

$$\dot{\mathbf{x}}(s,t) = \mathbf{F}^\perp(\mathbf{x}(s,t)), \tag{3.4}$$

$$\mathbf{x}(s,0) = \Gamma(s) \subset \partial\Omega, \tag{3.5}$$

where $\dot{\mathbf{x}} := \frac{\partial}{\partial t}\mathbf{x}$. Notice that

$$0 = \nabla \times (r\mathbf{F}) = -\mathbf{F}^\perp \cdot \nabla r + \big(\partial_x F^y - \partial_y F^x\big).$$

Therefore,

$$\frac{\partial}{\partial t} r(\mathbf{x}(s,t)) = \dot{\mathbf{x}}(s,t) \cdot \nabla r = \partial_x F^y - \partial_y F^x = \nabla \times \mathbf{F}(\mathbf{x}(s,t)).$$

We may find r by integrating the above from the boundary,

$$r(\mathbf{x}(s,t)) = r(\mathbf{x}(s,0)) \exp\left(\int_0^t \nabla \times \mathbf{F}(\mathbf{x}(s,\tau))\, d\tau \right), \tag{3.6}$$

where $\mathbf{x}(s,0) \in \Gamma \subset \partial\Omega$ and $r(\mathbf{x}(s,0))$ is the given boundary condition.

The curve $\mathbf{x}(s,\cdot)$ is called a *characteristic line*. One can easily see that this curve is an equipotential line since the current density $\mathbf{J}$ and the electrical field $\mathbf{E} = -\nabla u$ are parallel to each other for an isotropic conductivity case.

Remark 3.3 (Equipotential line method)**.** *The equipotential lines are easily obtained from* $\mathbf{J}$ *for an isotropic case. Since the voltage* u *is constant on it, one may compute the voltage first if the boundary voltage is given. Then, the conductivity is obtained by Ohm's law. We will call this algorithm the equipotential line method and related simulation images are in Figures 12 and 15 (see* [17]*).*

Remark 3.4 (Direct integration method)**.** *One may use the formula (3.6) to directly compute the resistivity along characteristic lines. Reconstructed conductivity images by such a direct integration are given in Figures 13 and 16. This is basically the same method used by Ider* et al. [13, Figure 6]*. If two sets of current data are given, the performance can be improved by integrating along non-characteristic lines (see* [13, Figure 4]*).*

3.4. **Noise propagation along characteristic lines.**

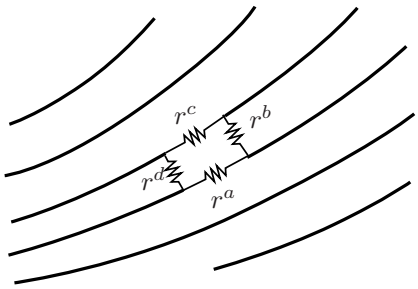

FIGURE 6. VRN and equipotential lines. If VRN is aligned along equipotential lines, the conductivity reconstruction process becomes more sensitive to noise.

Consider a case that the virtual network is aligned along characteristic lines as in Figure 6. Then, since there is no electrical current along equipotential lines, we have $F_a = F_c = 0$. Therefore, Eq. (3.1) becomes

$$r^b F^b - r^d F^d = 0 \quad \text{or} \quad r^b = r^d F^d / F^b.$$

Notice that only the information along the characteristic line is used to compute r^b and hence the domains of dependence and influence are restricted to the cells along the characteristic line. Therefore, the algorithm has no regularizing effect, and VRN becomes like the Direct Integration algorithm. In other words, it is important not to align the virtual

network system in a direction which is parallel to the equipotential lines. Rotating a network in the next section is one of the strategies to avoid such a situation locally.

4. VRN method based on stream functions

In the numerical simulations with regularized data we use a discretization method based on stream functions. In this way we may handle the data flexibly without discretization error. We briefly introduce the technique in this section.

4.1. **Stream function.**

Suppose that a current density $\mathbf{F}$ is given along network edges. If the network is rotated, one should reassign the current density along new edges by interpolating the given data. However, a new noise may appear in doing that and, more importantly, fundamental physical laws such as Kirchoff's current law can be broken. In this section we develop an interpolation method based on the *stream function* that keeps Kirchoff's current law valid.

We solve (2.6) to find a *stream function* ψ inside the domain Ω. Let $c = y^{j+1} - y^j = x^{i+1} - x^i$. Then, (2.6) is written as

$$\begin{aligned} cF^{i+\frac{1}{2}\,j} &= \psi^{i+\frac{1}{2}\,j+\frac{1}{2}} - \psi^{i+\frac{1}{2}\,j-\frac{1}{2}}, \quad 0 \le i < n,\ 0 < j < n, \\ -cF^{i\,j+\frac{1}{2}} &= \psi^{i+\frac{1}{2}\,j+\frac{1}{2}} - \psi^{i-\frac{1}{2}\,j+\frac{1}{2}}, \quad 0 < i < n,\ 0 \le j < n \end{aligned} \tag{4.1}$$

(see Figure 7). Notice that there are n^2 unknowns of $\psi^{i+\frac{1}{2}\,j+\frac{1}{2}}$ with $0 \le i, j < n$ and $2n(n-1)$ equations in (4.1) and hence the system is over determined. However, the sum of incoming current and outgoing current at a given vertex should be identical in a physically meaningful network, which is called Kirchoff's current law and written as

$$F^{i+\frac{1}{2}\,j} - F^{i-\frac{1}{2}\,j} + F^{i\,j+\frac{1}{2}} - F^{i\,j-\frac{1}{2}} = 0, \quad 0 < i, j < n. \tag{4.2}$$

Since the noised current density may not satisfy this relation, we should do the Helmholtz decomposition for the vector field and take the divergence free part (see Section 5.3.2). Notice that there are $(n-1)^2$ number of interior vertices and hence we have $(n-1)^2$ equations in (4.2). Therefore, the total number of independent equations are

$$2n(n-1) - (n-1)^2 = n^2 - 1.$$

Now there is one extra unknown left, which reflects the fact that the stream function is unique up to adding a constant. Hence we may ground it by using an extra equation $\psi^{\frac{1}{2}\,\frac{1}{2}} = 0$ and decide the stream function uniquely. The value of stream function along the outside of the domain can be solved by using the boundary current density (see Figure 7(a)). Notice that there are $4n$ exterior values for the stream function and $4n$ boundary edges. Hence, one can easily obtain them using the relations in (4.1).

Remark 4.1. *Notice that (4.1) is the network version of the relation* $\mathbf{F}^\perp = \nabla\psi$ *and (4.2) is the network version of zero divergence equation* $\nabla \cdot \mathbf{F} = \nabla \times \mathbf{F}^\perp = 0$. *Therefore, the existence of* $\psi^{i+\frac{1}{2}\,j+\frac{1}{2}}$ *is simply the network version of the existence of a potential.*

Remark 4.2. *The VRN based on stream function technique is equivalent to harmonic* B^z *algorithm. Let* $\mathbf{H}$ *be the magnetic field. Then, the fourth law of Maxwell's equation, or*

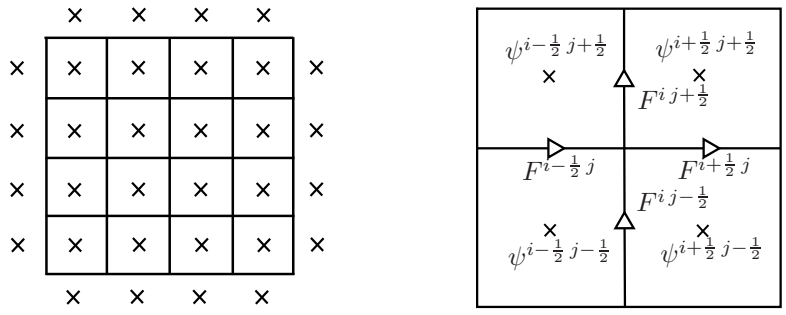

(a) ψ is defined at cell center (b) stream function and current

FIGURE 7. The points marked by $\times$ are where ψ is defined.

Ampere's law, is written as

$$\nabla \times \mathbf{H} = \mathbf{J}.$$

In two space dimensions, we have $\partial_z H^y = \partial_z H^x = 0$ *and hence*

$$\begin{pmatrix} J^x \\ J^y \end{pmatrix} = \begin{pmatrix} \partial_y H^z \\ -\partial_x H^z \end{pmatrix},$$

i.e., the stream function is the z-component of the magnetic field. It is the magnetic flux density $\mathbf{B} = \mu\mathbf{H}$ *that is measured by the MRI technology, where the coefficient* μ *is called the permeability. Therefore, for a two dimensional current flow, the mimetic approach in this paper is a way to reduce the intermediate data process and to minimise discretization error (see* [24] *and Appendix A).*

4.2. **Network rotation.**

In this section we consider a technique of rotating a network for two reasons. First, the relation (3.3) is applicable only if $F^b - F^c \ncong 0$. The choice of admissible boundary (see Section 3.1) gives a better chance to avoid such a situation. However, if the current density $\mathbf{F}$ contains a noise, the case of $F^b - F^c \cong 0$ may appear in any place. We expect such noise effects disappear in some regions by rotating the network. Another reason is to avoid a region that the network is parallel to the characteristic lines. In this way we may reduce the stripes of noises from reconstructed images. Notice that we may produce several conductivity images even with a single set of current data if different rotation angles are used. Comparing these images may help us to distinguish the effect of noise and true conductivity.

If a stream function for a given current density $\mathbf{F}$ is obtained, one is ready to rotate the network. In Figure 8(a) a network system is given before a rotation. In this example, the domain Ω of the conductivity body is the circular disk tangent to the outside square and is placed on the rectangular network. In Figure 8(b) this network system has been rotated with angle $\theta = 45°$. In that case the edges and the center of each cell represent different places of the body. Therefore, we should reassign the current data to each edge. To do this we first interpolate the values of the stream function at the new centers of rotated cells and then reassign the current along each edge by the relations in (4.1). In this way we may reduce discretization error and satisfy Kirchoff's current law. The purpose of network rotation is not to find the best angle of rotation, but to distinguish the effect

of noise and true conductivity by rotating a network with a relatively small angle. The network rotation gives a series of images for the static conductivity.

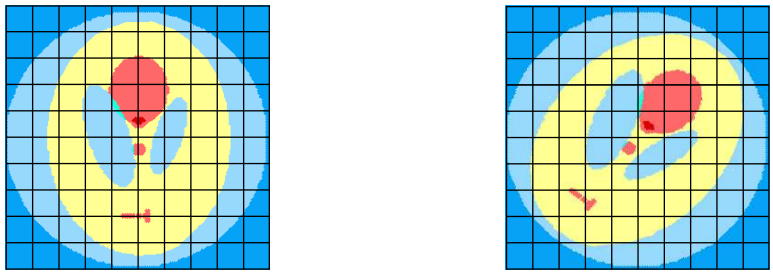

(a) network before rotation $\theta = 0$ (b) rotated body with $\theta = 45°$

FIGURE 8. If a network is rotated, the center of each cell is changed. The value of the stream function at these new cell centers is interpolated. The current density along a new edge is given by these values.

5. Numerical simulation

5.1. **Simulation setup.**

We took a target conductivity σ from a Matlab function for our numerical simulation, which is given in Figure 9. This image has been frequently used by many authors. The scale of the conductivity value is

$$0.1 \leq \sigma \leq 0.5,$$

where the range of corresponding resistivity is $2 \leq r \leq 10$. In the simulation we compute the resistivity distribution first using VRN method and then convert the images in terms of conductivity for an easier comparison to other methods. The challenging part of this target conductivity is the discontinuity that may parallel to the electrical current. The physical size of the conductivity body used in the simulation is a circular disk with the diameter of 50 centimeters.

The electrical current of $10mA$ was uniformly injected through the circular boundary in the second quadrant, $\frac{\pi}{2} \leq \theta \leq \pi$, where the origin is the center of the circular domain. The same amount of current is uniformly extracted from the boundary in the fourth quadrant, $-\frac{\pi}{2} \leq \theta \leq 0$. The boundary Γ^0 in Definition 2.1 consists of these two parts of current injection and extraction. The boundary in the first quadrant, $0 < \theta < \frac{\pi}{2}$, becomes Γ^+ and the one with $-\pi < \theta < -\frac{\pi}{2}$ is Γ^-. For the boundary condition we took $\Gamma = \overline{\Gamma^-}$. This boundary condition can be extended to Γ^0 exactly since the boundary itself is a characteristic line (see [19]). In fact we took the boundary data in the region $\frac{3\pi}{4} < \theta < \frac{7\pi}{4}$.

The exact current density $\mathbf{J}$ has been obtained by solving a forward problem using a network system, which are displayed in Figure 10. It is well known that the network forward solver is equivalent to a FDM forward solver (see Remark 3.2 or Strang [25]). The advantage of using network forward solver is to minimize discretization error. We have obtained a current density $\mathbf{J} = (J^x, J^y)$ with the size of

$$1.1 \times 10^{-3}\ [A/m] \leq\ |\mathbf{J}|\ \leq 4.6 \times 10^{-2}\ [A/m].$$

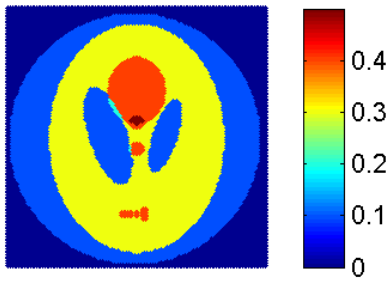

FIGURE 9. True conductivity image used in the simulation. The circular domain tangent to the outside square is used.

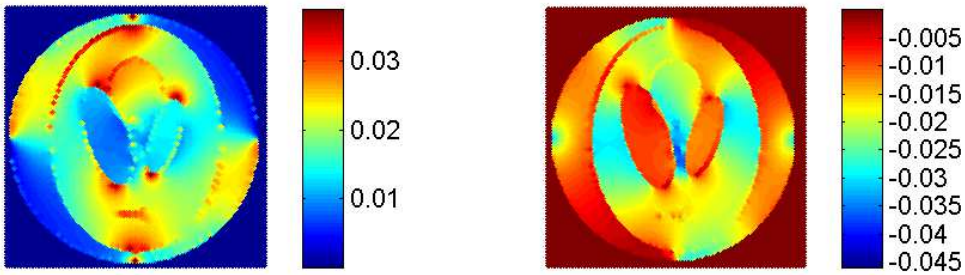

(a) J^x: x-component of current (b) J^y: y-component of current

FIGURE 10. The current $\mathbf{J}$ is obtained by solving the forward problem using 128×128 mesh grids. The number of cells inside the circular domain is 11,934.

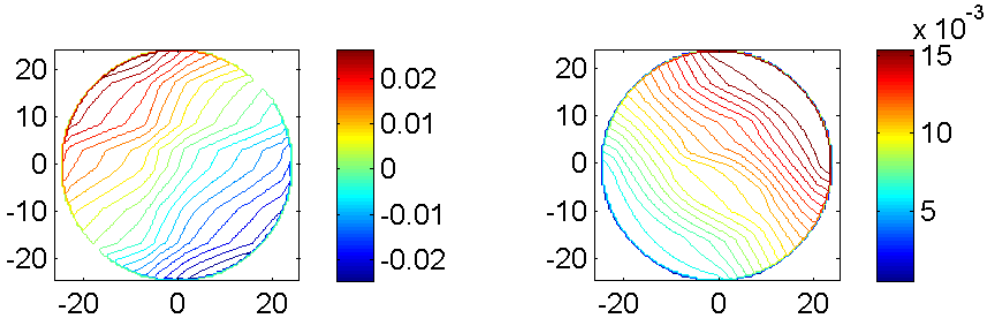

(a) equipotential lines (b) stream lines

FIGURE 11. The equipotential and stream lines of the current density $\mathbf{J}$.

The dimension $[A/m]$ of a current density fits to our two dimensional model. Using the relations in (4.1) and (4.2) we may compute the corresponding stream function ψ. In Figures 11(a) and (b), the equipotential lines and the stream lines are given, respectively. The streams lines are level curves of a corresponding stream function, which are perpendicular to equipotential lines.

5.2. **Multiplicative and additive noises.**

We add a noise to the current data in the following simulations to test the stability of algorithms. We add two kinds of noises, which will be called *multiplicative* and *additive*

noises. The multiplicative noise of $p\%$ is a random noise computed by

$$\left(\frac{p}{100}|\mathbf{J}(\mathbf{x})|\right) X,$$

where $-1 \leq X \leq 1$ is the random variable with a uniform distribution. The size of the multiplicative noise is proportional to the size of current $\mathbf{J}$.

The additive noise follows a normal distribution of average $\mu = 0$ and a standard deviation $s.d. > 0$, say $N(\mu = 0, s.d.)$. (Note that the standard deviation is usually denoted by σ, but we have already used it for conductivity.) Summing them up gives the current density data used in the simulation:

$$\mathbf{F} = \mathbf{J} + \left(\frac{p}{100}|\mathbf{J}|\right) X + N(0, s.d.). \tag{5.1}$$

As a measure of additive noise we consider the ratio of signal to standard deviation,

$$S/D := \frac{\text{averaged current } \underline{\text{S}}\text{ignal per edge}}{\text{standard } \underline{\text{D}}\text{eviation of noise}}. \tag{5.2}$$

There are $23,863$ network edges in the interior circular domain and the average current used in the simulation is about $0.078mA$. For example, in the second simulation of Figure 18 an additive noise with a standard deviation $s.d. = 0.003mA$ has been added to each of the edges and hence the ratio is $S/D \cong 26$.

5.3. **Comparison of reconstructed images.**

In this section we test the performance of the VRN method and compare it with the equipotential line method (Remark 3.3) and the direct integration method (Remark 3.4). In Section 5.3.1, we reconstruct the conductivity image from a noised current density without any noise regularization. This test shows clearly how a noise propagates. In Section 5.3.2 the noised data are regularized by convoluting them with a kernel and then taking the divergence free part of the Helmholtz decomposition. These three tested methods reconstruct the conductivity without iteration and hence the computation time is shorter than iterative ones. In Appendix A we also compare to the harmonic B^z MREIT method which is a widely used iterative method.

5.3.1. *Simulation before regularization.* The images in Figure 12 are reconstructed conductivity distributions obtained by the equipotential line method. One can clearly observe the stripes along equipotential lines from the reconstructed images. These show that the noise of current density along the equipotential lines stays in them. In Figure 13 the conductivity images have been reconstructed by the direct integration method given by the formula (3.6). These reconstructed images have the same structure as the ones by the equipotential line method. Notice that equipotential lines and characteristic lines are identical for the isotropic conductivity case and the noise inside a characteristic line stays in them. The performance of these two methods are compatible.

In Figure 14, reconstructed conductivity images by the VRN method are given. For the case with 1% multiplicative noise, the conductivity image has been almost exactly recovered. For the case with 5% noise, a wide and relatively thin band appears in the direction of characteristic lines. However, the narrow and thick stripes of the other methods have been disappeared and one may still observe the small and large anomalies in the domain. A problematic region is the left lower part of the domain. This is a region

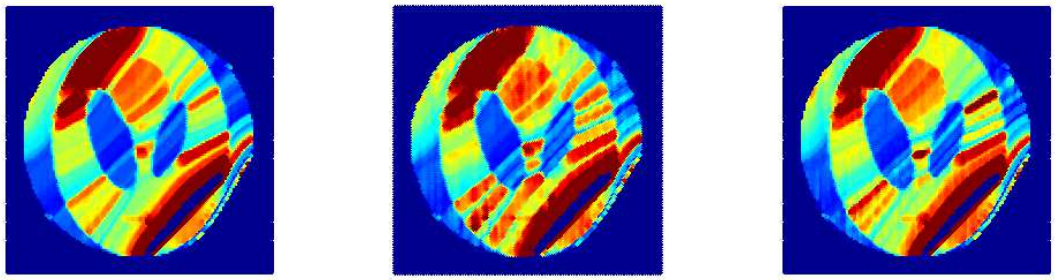

1% multiplicative noise 5% multiplicative noise additive, $S/D = 260$

FIGURE 12. Equipotential line method without a noise regularization

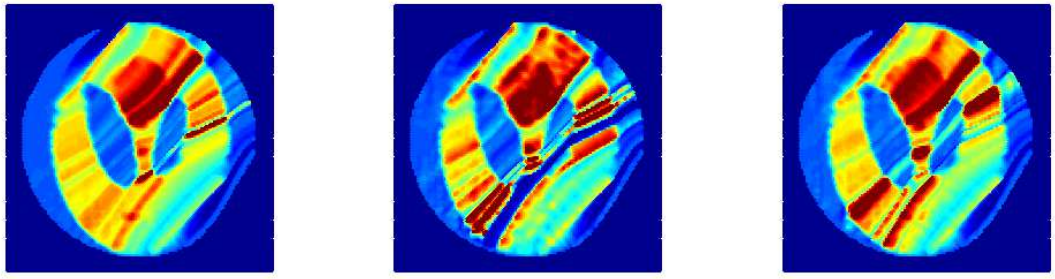

1% multiplicative noise 5% multiplicative noise additive, $S/D = 260$

FIGURE 13. Direct integration given in Eq. (3.6) without a noise regularization

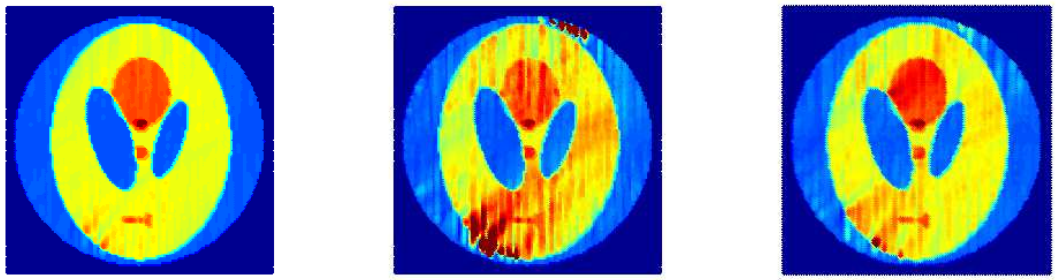

1% multiplicative noise 5% multiplicative noise additive, $S/D = 260$

FIGURE 14. Virtual Resistive Network (VRN) without a noise regularization

that the electrical current is parallel to the discontinuity lines of conductivity. The small anomalies in the lower middle regions of the domain are not observed because of this region. The problematic region remains with the added additive noise, too.

5.3.2. *Simulation after regularization.* In this section we reconstruct the conductivity image using regularized current data. We briefly explain the noise regularization method used in this section. First we smooth the noised data by convoluting them with a kernel given in matlab which averages 9 values of nearby cell with weights of

$$\begin{pmatrix} 0.0251 & 0.1453 & 0.0251 \\ 0.1453 & 0.3183 & 0.1453 \\ 0.0251 & 0.1453 & 0.0251 \end{pmatrix}.$$

Note that the current of a resistive network should satisfy Kirchoff's current law (4.2), which is equivalent to the zero divergence equation, $\nabla \cdot \mathbf{F} = 0$, in the continuum version. However, the noised data do not satisfy the relation. We decompose the data into the divergence free and curl free parts using the following Helmholtz decomposition algorithm. Set

$$\mathbf{F} = \begin{pmatrix} \partial_y \psi \\ -\partial_x \psi \end{pmatrix} + \begin{pmatrix} \partial_x \phi \\ \partial_y \phi \end{pmatrix},$$

where the first part is divergence free and the second one is curl free. Therefore,

$$\Delta \psi = -\nabla \times \mathbf{F}, \qquad \Delta \phi = \nabla \cdot \mathbf{F}, \quad x \in \Omega.$$

For the boundary condition, we take

$$\nabla \psi \cdot \mathbf{n}^{\perp} = g, \quad \nabla \phi \cdot \mathbf{n} = \mathbf{F} \cdot \mathbf{n} - g, \quad x \in \partial\Omega.$$

Notice that we only need ψ, which is a steam function. The normal component g of the boundary current is the one in (1.2), which has been chosen for the experiment.

Conductivity images in Figures 15 and 16 are obtained by the equipotential line and the direct integration methods, respectively. The reconstructed images are somewhat improved in compare with the ones in Figures 12 and 13 by using the regularized noised data. However, the improvement is not substantial and the overall properties of the two methods are not changed. The noise propagation property along the characteristic lines still gives severe damages to the image. On the other hand the images obtained by the VRN method have been improved substantially more when the regularized data is used. In fact one may obtain almost perfect conductivity imaged if the noise level are same as the above. Conductivity images in Figures 17 and 18 are obtained by the VRN method with increased noise levels. The three conductivity images in Figure 17 were obtained after adding multiplicative noises of $10, 20$ and 40%, respectively. The conductivity image is almost perfectly recovered when 10% multiplicative noise is added. One may still observe the stripes along the characteristic lines as the noise level increases. The three conductivity images in Figure 18 were obtained after adding additive noises of signal-deviation ratios $S/D = 78, 26$ and 16, respectively. One may similarly observe the improvement of recovered images with regularized current data. However, one may still observe noise propagation along the characteristic lines as the noise level increases.

6. Discussions

An isotropic conductivity reconstruction algorithm has been developed in this paper when the current density $\mathbf{J}$ is given in the whole domain. The motivation of this inverse problem is from the magnetic resonance imaging based electrical impedance tomography or simply MREIT. Many authors took the zero divergence equation (1.2) and the Ohm's law (1.3) to reconstruct the conductivity distribution. However, the Faraday's law (1.1) gives a direct relation between a current density, which is the choice of this paper. Discretization of this curl free equation has been studied relatively less than the divergence free equation. We have constructed a rectangular resistive network system to discretize the equation. Then, a contour integration on each rectangular cell boundary gives Kirchoff's voltage law. Using this network discretization the VRN (virtual resistive network) method suggested in this paper successfully reconstructed the conductivity image.

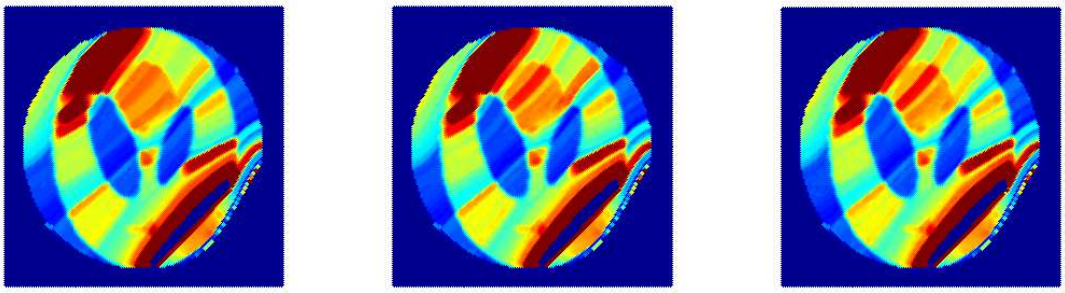

1% multiplicative noise 5% multiplicative noise 5%, $S/D = 260$

FIGURE 15. Equipotential line method with regularized noised data

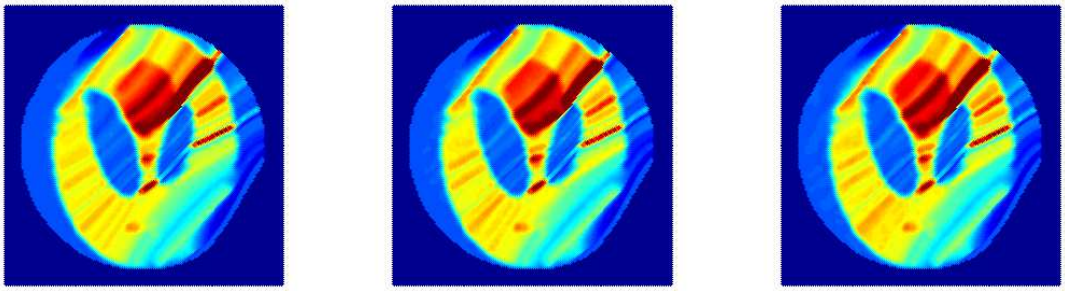

1% multiplicative noise 5% multiplicative noise 5%, $S/D = 260$

FIGURE 16. Direct integration given in Eq. (3.6) with regularized noised data

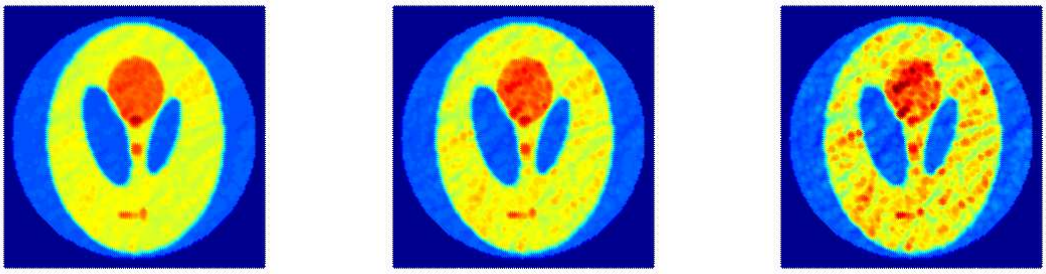

10% multiplicative noise 20% multiplicative noise 40% multiplicative noise

FIGURE 17. VRN method with regularized multiplicative noises

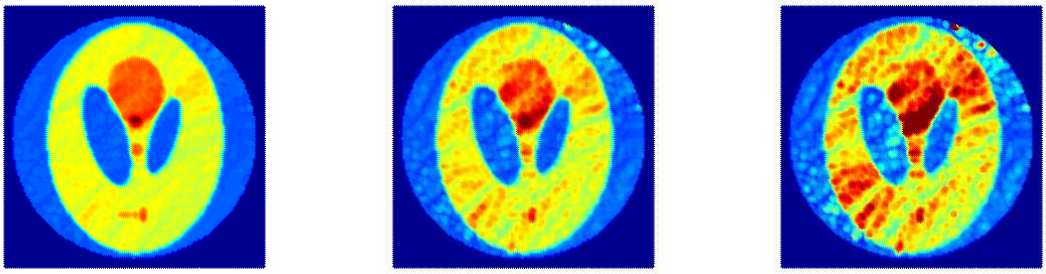

additive, $S/D = 78$ additive, $S/D = 26$ additive, $S/D = 16$

FIGURE 18. VRN method with regularized additive noises

The introduced VRN method has two important features. First, the reconstruction process depends only on local structure and is obtained by algebraic calculations in (3.3) for n^2 times. Notice that this computation is even simpler than solving the forward problem in (1.2), and that having a fast algorithm is crucial in a three dimensional computation. Second, the VRN method allows a larger noise level in compare with other methods. The maximum noise level we have tested is a 40% multiplicative noise or an additive noise of

$$S/D := \frac{\text{averaged current } \underline{\text{S}}\text{ignal per edge}}{\text{standard } \underline{\text{D}}\text{eviation of noise}} \cong 16.$$

The simulations in the paper indicate that the key to a successful conductivity reconstruction is reducing the noise effect that propagates along equipotential lines. The equipotential line and direct integration methods severely suffer because of it. The iterative harmonic B^z method is more robust than these methods (see Figure 19). The VRN method shows the most robust behavior among tested methods (see Figures 17 and 18). However, stripes along equipotential lines still appear as the noise level increases.

One way to reduce such a symptom is to take another set of current data with different direction of equipotential lines. Then, the noise propagation along characteristic lines can be cancelled to each other. In fact, Ider *et al.* have used two sets of current data to integrate the term in (3.6) along non-characteristic lines and successfully improved the conductivity image from [13, Figure 6] to [13, Figure 4] with a 10% multiplicative noise. The harmonic B^z algorithm is also designed to use two sets of B^z data for the same reason, where its reconstructed images are given in Figure 20 using two sets of current data. One may clearly observe the improvement in compare with the ones in Figure 19, which uses single set of current data. There are many red dots in the recovered conductivity image with 40% noise level. However, these dots are not aligned along equipotential lines. The resolution of this images is comparable to the one in Figure 17. However, the dots in Figure 17 are aligned along the characteristic lines since they are obtained single set of current data.

Appendix A. Harmonic B^z algorithm (an iterative method)

The VRN method introduced in this paper is a non-iterative method and has been compared with two other non-iterative methods. The advantages of non-iterative method are the low computational cost and being free of convergence issues caused by iteration arguments. On the other hand iterative methods have the advantage of flexibility. The harmonic B^z MREIT algorithm [24] is a widely used method which has been successful with experimental data. The original idea of the algorithm is to reconstruct the conductivity image with two sets of B^z data without measuring other two components of the magnetic field, which is a big advantage in handling real experiments. In two space dimensions, this B^z data are enough to obtain the electrical current, and hence the harmonic B^z algorithm and the J-substitution method (see [16]) become equivalent.

The algorithm is based on iterative arguments. Let $\sigma^1 = 1$ and σ^n be obtained in the algorithm. To obtain σ^{n+1}, one should first solve the forward problem (1.2) with the given conductivity $\sigma = \sigma^n$. Then, σ^{n+1} is obtained from the relation (1.3), i.e., $\sigma^{n+1} := \frac{|\mathbf{F}|}{|\nabla u|}$. In Figure 19 reconstructed conductivity images are given after a normalization. These are the images obtained after 20 iterations when the variation stays within a toleration range.

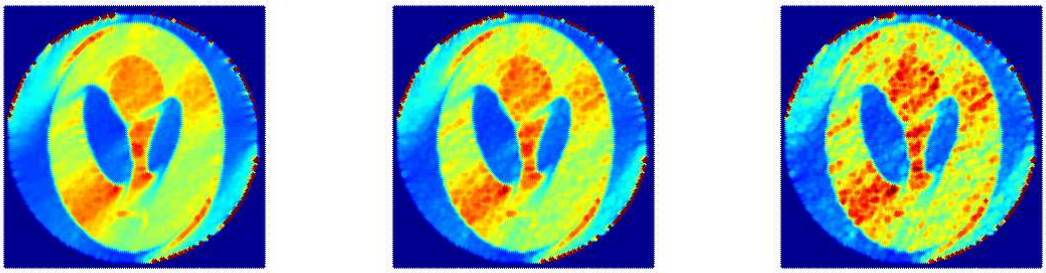

10% multiplicative noise 20% multiplicative noise 40% multiplicative noise

FIGURE 19. Harmonic B^z method with single set of regularised noised data

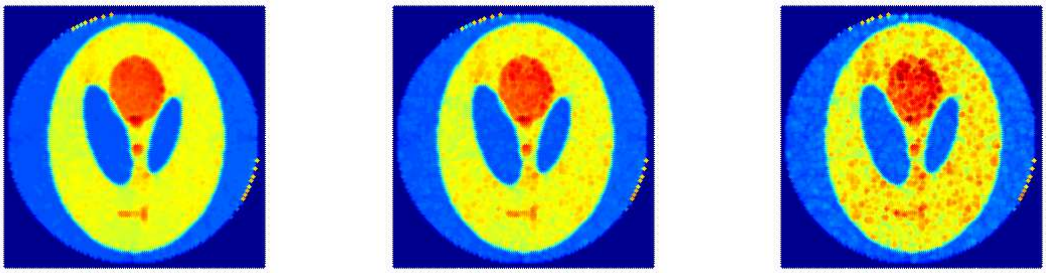

10% multiplicative noise 20% multiplicative noise 40% multiplicative noise

FIGURE 20. Harmonic B^z method with two sets of regularised noised data

This method is less sensitive in the noise propagation along the characteristic lines than the two compared methods. However, as the noise level increases, the stripes still appear and the images obtained by the VRN method in Figure 17 show a better resolution.

Notice that the harmonic B^z algorithm is originally designed to use two sets of data. Let $\mathbf{F}_1$ and $\mathbf{F}_2$ be two given current data. Then, the conductivity is updated by alternating the two data as $\sigma^{2n} := \frac{|\mathbf{F}_2|}{|\nabla u|}$ and $\sigma^{2n+1} := \frac{|\mathbf{F}_1|}{|\nabla u|}$. Reconstructed images are given in Figure 20, where the second current was obtained after rotating the boundary current by 90 degree. One can see the considerable improvement and the stripes along the equipotential lines are all disappeared. The image quality is now similar to the one in Figure 17, which were obtained by the VRN method with single set of current data.

REFERENCES

[1] Habib Ammari, *An introduction to mathematics of emerging biomedical imaging*, Mathématiques & Applications (Berlin) [Mathematics & Applications], vol. 62, Springer, Berlin, 2008. MR 2440857 (2010j:44002)

[2] Habib Ammari, Yves Capdeboscq, Hyeonbae Kang, and Anastasia Kozhemyak, *Mathematical models and reconstruction methods in magneto-acoustic imaging*, European J. Appl. Math. **20** (2009), no. 3, 303–317. MR 2511278 (2010f:35428)

[3] Habib Ammari, Josselin Garnier, and Knut Sølna, *Partial data resolving power of conductivity imaging from boundary measurements*, SIAM J. Math. Anal. **45** (2013), no. 3, 1704–1722. MR 3061470

[4] ———, *Resolution and stability analysis in full-aperture, linearized conductivity and wave imaging*, Proc. Amer. Math. Soc. **141** (2013), no. 10, 3431–3446. MR 3080166

[5] Habib Ammari and Hyeonbae Kang, *Reconstruction of small inhomogeneities from boundary measurements*, Lecture Notes in Mathematics, vol. 1846, Springer-Verlag, Berlin, 2004. MR 2168949 (2006k:35295)

[6] Douglas N. Arnold, Pavel B. Bochev, Richard B. Lehoucq, Roy A. Nicolaides, and Mikhail Shashkov (eds.), *Compatible spatial discretizations*, The IMA Volumes in Mathematics and its Applications, vol. 142, Springer, New York, 2006, Papers from the IMA Hot Topics Workshop on Compatible Spatial Discretizations for Partial

Differential Equations held at the University of Minnesota, Minneapolis, MN, May 11–15, 2004. MR 2256572 (2007c:65004)

[7] Douglas N. Arnold, Richard S. Falk, and Ragnar Winther, *Finite element exterior calculus, homological techniques, and applications*, Acta Numer. **15** (2006), 1–155. MR 2269741 (2007j:58002)

[8] ———, *Finite element exterior calculus: from Hodge theory to numerical stability*, Bull. Amer. Math. Soc. (N.S.) **47** (2010), no. 2, 281–354. MR 2594630 (2011f:58005)

[9] Pavel B. Bochev and James M. Hyman, *Principles of mimetic discretizations of differential operators*, Compatible spatial discretizations, IMA Vol. Math. Appl., vol. 142, Springer, New York, 2006, pp. 89–119. MR 2249347 (2007k:65161)

[10] Liliana Borcea, *Electrical impedance tomography*, Inverse Problems **18** (2002), no. 6, R99–R136. MR 1955896

[11] Soo Yeol Lee Eung Je Woo and Chi Woong Mun, *Impedance tomography using internal current density distribution measured by nuclear magnetic resonance*, Proc. SPIE **2299** (1994), 377–85.

[12] Y.Z. Ider and S. Onart, *Algebraic reconstruction for 3D magnetic resonance electrical impedance tomography (MREIT) using one component of magnetic flux density*, Physiological measurement **25** (2004), 281.

[13] Y.Z. Ider, S. Onart, and W. Lionheart, *Uniqueness and reconstruction in magnetic resonance-electrical impedance tomography (MR-EIT)*, Physiological measurement **24** (2003), 591–604.

[14] Ohin Kwon Jin Keun Seo and Eung Je Woo, *Magnetic resonance electrical impedance tomography (MREIT): conductivity and current density imaging*, Journal of Physics: Conference Series **12** (2005), 140.

[15] H.S. Khang, B.I. Lee, S.H. Oh, E.J. Woo, S.Y. Lee, M.H. Cho, Kwon O., Yoon J.R., and J.K. Seo, *J-substitution algorithm inmagnetic resonance electrical impedance tomography (mreit): phantom experiments for static resistivity images*, IEEE Trans. Med. Imaging **21** (2002), 695–702.

[16] Yong Jung Kim, Ohin Kwon, Jin Keun Seo, and Eung Je Woo, *Uniqueness and convergence of conductivity image reconstruction in magnetic resonance electrical impedance tomography*, Inverse Problems **19** (2003), no. 5, 1213–1225.

[17] Ohin Kwon, June-Yub Lee, and Jeong-Rock Yoon, *Equipotential line method for magnetic resonance electrical impedance tomography*, Inverse Problems **18** (2002), no. 4, 1089–1100.

[18] Ohin Kwon, Eung Je Woo, Jeong-Rock Yoon, and Jin Keun Seo, *Magnetic resonance electrical impedance tomography (MREIT): simulation study of J-substitution algorithm*, Biomedical Engineering, IEEE Transactions on **49** (2002), no. 2, 160 –167.

[19] Min-Gi Lee and Yong-Jung Kim, *Well-posedness of the conductivity reconstruction from an interior current density in terms of schauder theory*, Quart. Appl. Math. (To appear).

[20] Tae Hwi Lee, Hyun Soo Nam, Min Gi Lee, Yong Jung Kim, Eung Je Woo, and Oh In Kwon, *Reconstruction of conductivity using the dual-loop method with one injection current in MREIT*, Physics in Medicine and Biology **55** (2010), no. 24, 7523.

[21] Carlos Montalto and Plamen Stefanov, *Stability of coupled-physics inverse problems with one internal measurement*, Inverse Problems **29** (2013), no. 12, 125004, 13. MR 3129114

[22] Adrian Nachman, Alexandru Tamasan, and Alexandre Timonov, *Recovering the conductivity from a single measurement of interior data*, Inverse Problems **25** (2009), no. 3, 035014, 16. MR 2480184 (2010g:35340)

[23] A.I. Nachman, *Global uniqueness for a two-dimensional inverse boundary value problem*, Annals of Mathematics (1996), 71–96.

[24] Jin Keun Seo and Eung Je Woo, *Magnetic resonance electrical impedance tomography (MREIT)*, SIAM Review **53** (2011), no. 1, 40–68.

[25] Gilbert Strang, *Introduction to applied mathematics*, Wellesley-Cambridge Press, Wellesley, MA, 1986.

[26] J. Sylvester and G. Uhlmann, *A global uniqueness theorem for an inverse boundary value problem*, Annals of Mathematics (1987), 153–169.

[27] E. J Woo and J. K Seo, *Magnetic resonance electrical impedance tomography (MREIT) for high-resolution conductivity imaging*, Physiological Measurement **29** (2008), R1.

[28] Nanping Zhang, *Electrical impedance tomography based on current density imaging*, Master's Thesis, University of Toronto (1992).

Department of Mathematical Sciences, KAIST, 291 Daehak-ro, Yuseong, Daejeon 305-701, Korea
E-mail address: mgleemail@gmail.com, minsu.ko@kaist.ac.kr, yongkim@kaist.edu